ADVANCED MATERIALS INTERFACES
Open Access
www.advmatinterfaces.de

Comparison of Fabrication Methods for Fiber-Optic Ultrasound Transmitters Using Candle-Soot Nanoparticles

Semyon Bodian, Esra Aytac-Kipergil, Shaoyan Zhang, India Lewis-Thompson, Sanjayan Sathasivam, Sunish J. Mathews, Erwin J. Alles, Edward Z. Zhang, Paul C. Beard, Ross J. Gordon, Paul Collier, Ivan P. Parkin, Adrien E. Desjardins, Richard J. Colchester, and Sacha Noimark*

Candle-soot nanoparticles (CSNPs) have shown great promise for fabricating optical ultrasound (OpUS) transmitters. They have a facile, inexpensive synthesis whilst their unique, porous structure enables a fast heat diffusion rate which aids high-frequency ultrasound generation necessary for high-resolution clinical imaging. These composites have demonstrated high ultrasound generation performance showing clinically relevant detail, when applied as macroscale OpUS transmitters comprising both concave and planar surfaces, however, less research has been invested into the translation of this material's technology to fabricate fiber-optic transmitters for image guidance of minimally invasive interventions. Here, are reported two fabrication methods of nanocomposites composed of CSNPs embedded within polydimethylsiloxane (PDMS) deposited onto fiber-optic end-faces using two different optimized fabrication methods: "All-in-One" and "Direct Deposition." Both types of nanocomposite exhibit a smooth, black domed structure with a maximum dome thickness of 50 µm, broadband optical absorption (>98% between 500 and 1400 nm) and both nanocomposites generated high peak-to-peak ultrasound pressures (>3 MPa) and wide bandwidths (>29 MHz). Further, high-resolution (<40 µm axial resolution) B-mode ultrasound imaging of ex vivo lamb brain tissue demonstrating how CSNP-PDMS OpUS transmitters can allow for high fidelity minimally invasive imaging of biological tissues is demonstrated.

1. Introduction

Highly optically absorbing composite films have broad applicability in fields including actuation,[1–3] solar cells,[4–6] and biological[7] and gas sensing.[8] They can be deposited onto substrates with varying sizes[1,9] and geometries and patterned using techniques such as soft lithography.[2] Recently, these composites have shown significant promise for the biomedical imaging application, optical ultrasound (OpUS) generation.[10–13] OpUS generation describes the absorption of pulsed or modulated light by a material and subsequent generation of ultrasound through the photoacoustic effect.[14,15]

OpUS transmitters are well suited for biomedical ultrasound imaging due to their potential to provide wide acoustic bandwidths using short laser pulses[9] as well as their immunity to electromagnetic fields.[16–19] Materials developed for OpUS generation typically comprise an optically absorbing component embedded within optically transparent elastomeric

S. Bodian, E. Aytac-Kipergil, S. Zhang, I. Lewis-Thompson, S. J. Mathews, E. J. Alles, E. Z. Zhang, P. C. Beard, A. E. Desjardins, R. J. Colchester, S. Noimark
Department of Medical Physics and Biomedical Engineering
University College London
London WC1E 6BT, UK
E-mail: simon.bodian.13@ucl.ac.uk

The ORCID identification number(s) for the author(s) of this article can be found under https://doi.org/10.1002/admi.202201792.

DOI: 10.1002/admi.202201792

S. Bodian, E. Aytac-Kipergil, S. Zhang, I. Lewis-Thompson, S. J. Mathews, E. J. Alles, P. C. Beard, A. E. Desjardins, R. J. Colchester, S. Noimark
Wellcome/ESPRC Centre for Surgical and Interventional Sciences
University College London
Charles Bell House, 67–73 Riding House Street, London W1W 7EJ, UK

S. Bodian, S. Sathasivam, I. P. Parkin, S. Noimark
Materials Chemistry Centre
Department of Chemistry
University College London
20 Gordon Street, London WC1H 0AJ, UK

S. Sathasivam
School of Engineering
London South Bank University
London SE1 0AA, UK

R. J. Gordon, P. Collier
Johnson Matthey Technology Centre
Sonning Common, Reading RG4 9NH, UK

materials.[20] The former absorbs the incident pulsed laser light, generating heat. This thermal energy is then transferred to the elastomer and ultrasound is generated by the composite. The generated ultrasound pressure is directly proportional to the composite's volumetric thermal expansion coefficient.[21] A common elastomer used is polydimethylsiloxane (PDMS), employed for its chemical inertness, optical transparency, and large volumetric expansion coefficient.

Using a range of film deposition techniques, composites for OpUS have been applied onto macro[22–24] and microscale[9,11,25] substrates with planar and more challenging geometries. Most notably, much research has focused on developing low-cost, consistent fabrication methods to apply these composites onto the distal end of sub-millimeter optical fiber, transforming them into miniaturized OpUS transmitters.[25,26–29] Due to their small size, they can be integrated into medical devices used for minimally invasive surgical interventions.[15–18] Taking advantage of these benefits, high-resolution ex vivo and in vivo ultrasound imaging of various tissues have been demonstrated using OpUS transmitters.[9,11,30]

A large range of optical absorbers for OpUS composites have been investigated including carbonaceous materials such as multiwall carbon nanotubes (MWCNTs),[9,25,31] carbon black,[24,32] graphene,[33] and carbon nanofibers[27] in addition to the organic dye crystal violet[11] and nanomaterials[24] such as gold nanoparticles (NPs)[34,35] and $CuInS_2$ quantum dots.[36] PDMS-based composites created using MWCNTs have been applied onto substrates ranging from macroscale planar substrates and curved surfaces to highly-miniature optical fibers. In particular, miniaturized OpUS transmitters designed using MWCNT-PDMS composite-coated optical fibers have demonstrated high photoacoustic conversion efficiencies, achieving high ultrasound pressures and wide frequency bandwidths. Coupled with a fiber-optic Fabry–Perot (FP) hydrophone,[37,38] these miniature transmitters have achieved high-resolution ultrasound imaging of ex vivo tissue, showing clinically relevant information.[9,25] Moreover, these miniaturized devices have demonstrated real-time, through-needle image-guidance of a cardiovascular intervention in vivo, in a pre-clinical model.[9,11,30]

Recently, candle-soot nanoparticles (CSNPs) have emerged as a promising broadband optical absorber for OpUS[39–41] due to several key benefits. First, their 3D hierarchical nanostructure provides their CSNP-PDMS composites with a low interfacial thermal resistance, manifesting in a fast heat diffusion rate.[18,32,36,37] This enables the temperature profile within the composite to resemble that of the input optical pulse which aids high-frequency ultrasound generation.[39] Second, they can be readily fabricated using a simple scalable and inexpensive facile synthesis.[19,39,42–44] Also, they can be applied onto both curved and planar macroscale substrates.[18,44–47] For example, CSNP-PDMS composites were applied onto concave substrates such as lenses, for use in high intensity focused ultrasound,[18,19,45,48] a therapeutic modality with wide-ranging medical applications including tumor therapy,[49] drug delivery,[50,51] and tissue ablation.[52,53] Many studies that have focused on developing CSNP composites for OpUS generation have demonstrated promising results when these composites have been produced as free-standing membranes. However, to date, only one study about CSNP-PDMS fiber-optic OpUS transmitters[47] has been reported in the literature.

There is a need for more development and investigation into both the fabrication and performance of fiber-optic OpUS transmitters featuring CSNP-PDMS composites to achieve large tissue penetration depths and high spatial resolution ultrasound imaging. To address this need, in this paper, we present and compare two facile and reproducible fabrication methods, a novel one-step fabrication method, which we term "All-in-One" (AiO), in addition to a previously reported fabrication strategy,[47] "Direct Deposition" (DD). Fiber-optic transmitters from both methods generated peak-to-peak ultrasound pressures above 3 MPa and bandwidths beyond 29 MHz, recording high-resolution ex vivo pulse-echo ultrasound images of lamb brain tissue at imaging depths of up to 10 mm. To the authors' knowledge, these ultrasound images of brain tissue are the first to be recorded ex vivo using OpUS imaging.

2. Experimental Section

2.1. Optical Fiber Preparation

All ultrasound transmitters were fabricated using step-index, silica-core, silica-cladding multimode fibers (FG200LCC, Thorlabs, Germany) with a Numeric Aperture: 0.22 and core/cladding diameters of 200/240 µm. Each fiber end-face was prepared by cleaving the fiber using an automated fiber cleaver (CT-100, Fujikura, Japan).

2.2. Polymer Preparation

For both CSNP-PDMS composite fabrication methods, namely, DD and AiO, the PDMS used was Sylgard 184 (Dow Corning, Europe), prepared by manually mixing the Sylgard elastomer base and curing agent (10:1 volumetric ratio), after which it was degassed under vacuum conditions (3 min).

2.3. All-In-One Fabrication

To synthesize CSNPs for AiO composites, a candle was assembled and lit, with a glass microscope slide clamped ≈2.5 mm above the candlewick. The candle was moved laterally within a flame by hand for around 3.5 min, to create a coating on the slide. Note that each position of the slide was exposed to the flame for 20 s, prior to translation. Subsequently, the slide was unclamped and the CSNPs were scraped off using a spatula, after which they were transferred into a pre-weighed vial. This process was repeated until a desired weight of CSNPs had been synthesized. CSNPs were then mechanically mixed with PDMS (30 mg:0.11 mL, CSNPs:PDMS) until a homogenous composite solution formed (Figure S7, Supporting Information). The optimal ratio of CSNPs to PDMS for OpUS was determined empirically through trial-and-error methods whereby the chosen ratio created a homogenous formulation which

ADVANCED MATERIALS INTERFACES
Open Access
www.advmatinterfaces.de

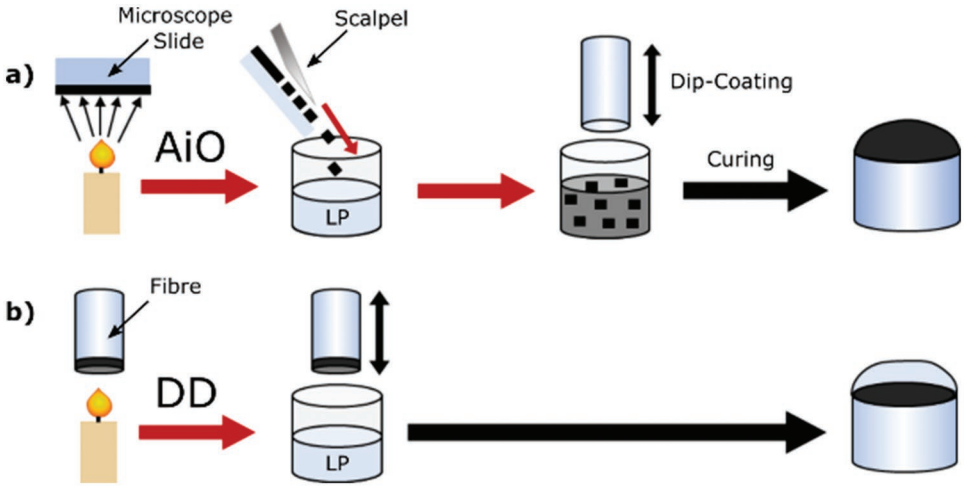

Figure 1. Schematic illustrating the Direct Deposition (DD) and AiO fabrication methods used to prepare CSNP-PDMS composites on optical fibers. a) For AiO composites, the candle-soot (black) is first deposited onto a glass microscope slide, after which it is manually transferred into a liquid PDMS (LP) solution and mechanically mixed. An optical fiber is then dip-coated into the CSNP-PDMS composite solution and allowed to cure in an upright position at room temperature, creating an AiO composite at the fiber distal end. b) For DD composites, the candle soot is directly deposited onto a fiber end face. The coated fiber is subsequently dip-coated with PDMS and allowed to cure in an upright position at room temperature, creating a bilayer CSNP-PDMS composite.

translated to uniform coverage of the fiber distal face after dip-coating. A prepared fiber was dip-coated in an optimized CSNP-PDMS composite solution and allowed to cure (48 h) with the distal end facing upright (**Figure 1**a). Using the AiO method, more than five optical fibers were coated with a CSNP-PDMS nanocomposite film.

3. Direct Deposition Fabrication

To synthesize CSNP films for DD composites, a prepared fiber was positioned within a candle flame, at a distance of 2.5 mm above the candlewick and held there for ≈4 s. The fiber was then overcoated with PDMS using a dip-coating method, producing a "bottom-up" CSNP-PDMS bilayer composite (Figure 1b). Using the DD method, more than five optical fibers were coated with CSNP-PDMS nanocomposite films.

4. Characterization

4.1. Composite Characterization

All fiber-optic composites were imaged using a stereomicroscope (IC80 HD, Leica, UK). The distal ends of the fibers were examined using "end-on" illumination as well as "through-fiber" illumination to highlight the composite surface topology and uniformity. In addition, the side-on imaging enabled inspection of composite thickness and geometry. Scanning electron microscopy (SEM) of the synthesized CSNPs, as well as all CSNP-PDMS composites on the distal ends of the optical fibers, were performed using secondary electron imaging with a field emission instrument (JSM-6301F, JEOL, Japan; acceleration voltage: 5.0 kV).

4.2. Optical and Ultrasound Characterization

The optical absorption of the CSNP-PDMS composites on the distal ends of optical fibers was measured across a wavelength range (400–1400 nm). Broadband light from a halogen lamp (HL-2000-HP-FHSA, Ocean Optics, USA) was delivered from the proximal end of a fiber and the light transmitted through the composite at the distal end was received in an integrating sphere (FOIS-1, Ocean Optics, USA) and measured with two spectrometers (Flame-T-VIS-NIR, 300–1000 nm and NIR-Quest512, Ocean Optics, USA, 1000–1800 nm). A non-coated cleaved fiber was used as a reference fiber, and dark measurements were taken to correct for background light.

Ultrasound was generated with pulsed laser light (1064 nm) generated by a Q-switched Nd:YAG laser (SPOT-10-500-1064, Elforlight, UK) with a pulse length of 2 ns, pulse energy of 25 μJ, and a repetition rate of 100 Hz. The corresponding laser fluence measured was 80 mJ cm^{-2}. The fibers were submerged within a water bath and measurements were taken with a needle hydrophone (NH0200, Precision Acoustics, UK; diameter = 200 μm, calibration range: 1–30 MHz) at an axial position of 1.5 mm from the fiber end-face centered on the generated ultrasound beam. The ultrasound generation of multiple coated fibers prepared using both the DD and AiO fabrication methods was measured, to obtain average values of the generated pressures and bandwidths along with corresponding standard deviations.

4.3. All-Optical Ultrasound Imaging

All-optical pulse-echo ultrasound imaging was accomplished by aligning an optical fiber coated with a CSNP-PDMS composite fabricated using the DD method alongside an OpUS

receiver comprising a plano-concave microresonator located on the distal tip of a single-mode optical fiber,[37,38] to form an OpUS imaging probe (Figure 6a). The design and fabrication of plano-concave microresonator have been described in a previous work.[37] In brief, a dielectric mirror (98% reflectivity) was deposited on the end face of the fiber, then the fiber was dip-coated with an epoxy dome, followed by coating with a second dielectric mirror (98% reflectivity). Subsequently, an outer coating of Parylene C was deposited on the distal tip of the fiber for protection. The fiber-optic ultrasound imaging probe was controlled and interrogated using a console for ultrasound generation and reception, which has been previously described.[30] The same laser was used for OpUS generation during imaging as employed for ultrasound characterization. For the ultrasound reception, a tunable continuous wave (CW) laser (Tunics T100S CL, Yenista Optics, France), working at a wavelength range of 1500–1600 nm, was used to interrogate the plano-concave microresonator. The laser was coupled to the fiber-optic plano-concave microresonator via a circulator and the reflected signal was monitored with a photodetector. The photodetector split the signal into low frequency (<50 kHz) and high-frequency (>500 kHz) components. The low-frequency component of the signal (<50 kHz) was digitized at 16 bits with a sampling rate of 1 MS s^{-1} (PCI-6251, National Instruments, UK) and was used to record the transfer function of plano-concave microresonator, whilst the high-frequency component (>500 kHz) was encoded with the received ultrasound signal[46] and digitized at 14 bits with a sampling rate of 100 MS s^{-1} (PCI-5142, National Instruments, UK).

The transducer probe was attached to a translational stage (Thorlabs, MTS50/M-Z8E) and the probe was lowered into a water bath above the imaged target and translated laterally across the target in 50 µm-sized steps. Prior to the display of the ultrasound images, a series of data processing steps were undertaken. Briefly, the image data were band-pass filtered (Butterworth, 4th order, 10–40 MHz) to suppress the noise. The low cut-off of 10 MHz was chosen to remove the low ultrasound frequencies which contribute to signal broadening and beam divergence, reducing the achievable lateral resolution.[20,54] Cross-talk originating from direct transmission of ultrasound from the CSNP-PDMS composite surface to the ultrasound receiver was then removed through a general linear model[9] and then processed by digital time gain compensation to reduce the impact of wave attenuation. Subsequently, synthetic aperture imaging was performed by concatenating processed signals from different locations which then underwent *k*-space reconstruction using the *k*-Wave toolbox.[55] Finally, the data underwent envelope detection with Hilbert transform and log compression was applied for display. The dynamic range of each ultrasound image was calculated as follows:

$$\text{Dynamic Range} = 20\log\left(\frac{\max}{\min}\right) \quad (1)$$

where "max" and "min" refer to the maximum and minimum reflected ultrasound intensity.

To measure both the axial and lateral resolutions of the imaging system, a phantom comprising multiple tungsten wires (27 µm diameter) which were mounted horizontally, was placed parallel to the water surface and imaged by translating the imaging probe 30 mm in 600 steps perpendicular to the probe translation axis. The tungsten wires were positioned at 12 depths relative to the ultrasound transmitter, ranging from 3 to 14 mm, with a 1 mm increment. To measure the spatial resolution provided by the probe, axial and lateral cross sections were then taken through the maximum of the point spread function from each tungsten wire image and the corresponding resolutions were calculated from the cross sections' full-width-at-half-maximum.

To demonstrate the ultrasound imaging capabilities of the imaging probe and that of the overall imaging system, ex vivo imaging was carried out on lamb brain tissue including cerebellum and cerebrum. The tissue was procured fresh and stored refrigerated. All imaging was carried out within 24 h of the animal being terminated. For imaging, the lamb's cerebellum and cerebrum were affixed to a mount with superglue in a water bath (Figure 6a) and image acquisition was executed by translating the probe across 25 mm using the motorized stage, with 500 lateral steps across the imaging region. The acquired images were processed with the same protocol described above. Following the imaging of the tissue, both the cerebellum and cerebrum were sectioned, imaged with a stereomicroscope, and fixed in formalin.

5. Results

5.1. Composite Characterization

Examination of the CSNP-PDMS fiber-optic composites using optical microscopy in combination with light delivery through the proximal end of the fiber indicated that both DD and AiO fabrication methods achieved uniform, optically absorbing composites, with smooth surfaces (**Figure 2**a,b,d,e). The CSNP-PDMS composites fabricated using the AiO and DD methods displayed similar average maximum dome thicknesses of 54.7 ± 1.71 and 51.8 ± 0.95 µm, respectively, with each composite's average thickness lying within the standard deviation of the other. Planar microscope slides exposed to the same candle flame for a time period of 5 s, slightly more than that of the fiber-optic end-face in the DD method, yielded a resulting CSNP layer thickness measured at 16.2 µm. Microscope examination indicated that in both cases, the resultant CSNP-PDMS composites are dome-shaped (Figure 2c,f) and those created using both fabrication methods transmitted under 1% of the incident light. SEM images showed that the AiO fabrication method results in composites that feature a textured, rough surface, in contrast to the smooth composite surface obtained using DD fabrication methods (**Figure 3**a,b). Moreover, SEM imaging highlighted the extensive 3D hierarchical structures of the candle-soot when deposited directly onto the glass substrate (Figure 3c,d).

5.2. Optical and Ultrasound Characterization

The optical absorption spectra of all CSNP-PDMS composites feature wide absorption profiles. Both fabrication methods resulted in composites with high optical absorption (>99%) across the wavelength range of 400–1200 nm (**Figure 4**a).

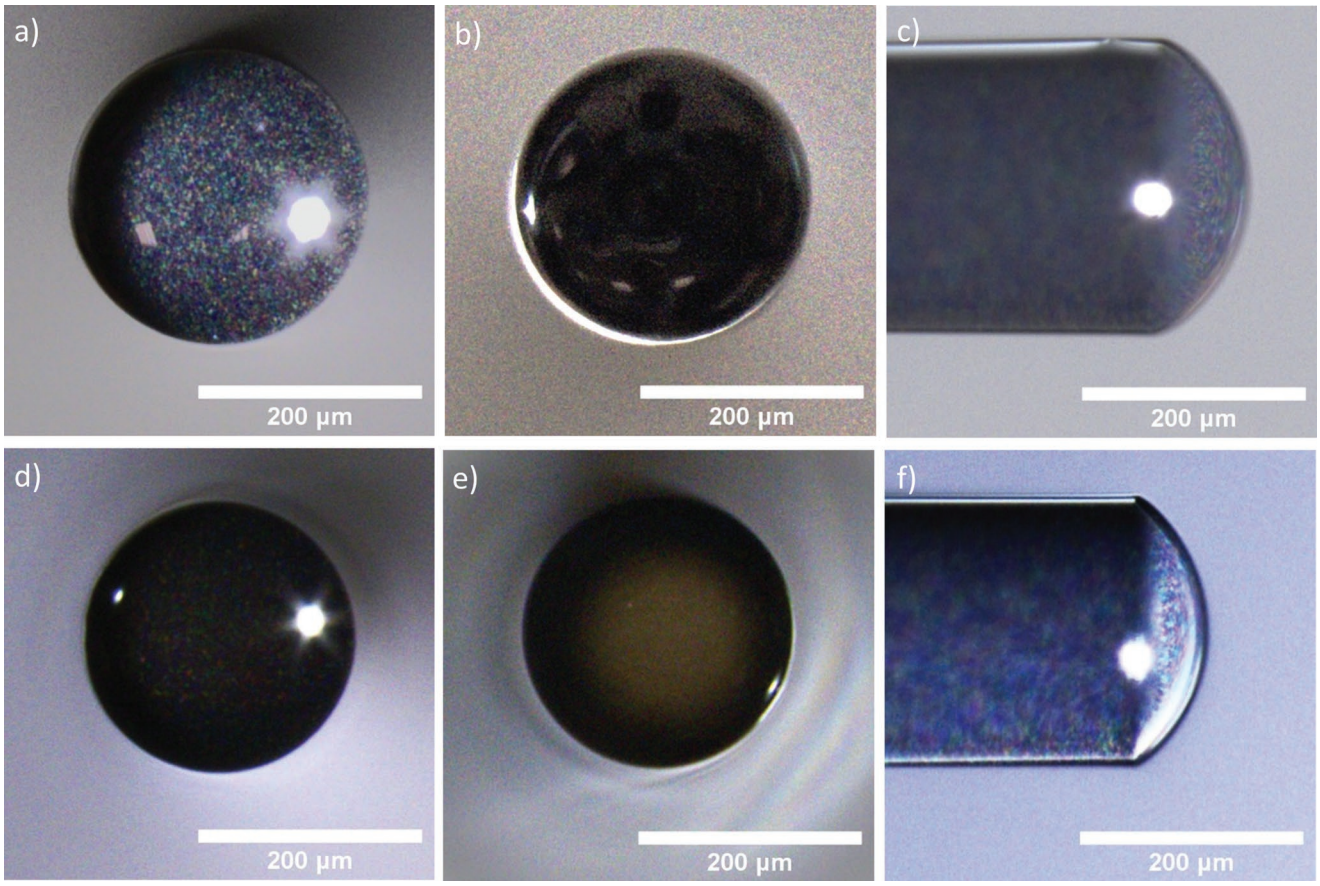

Figure 2. Stereomicroscope images of CSNP-PDMS coated optical fibers (diameter: 200 µm) prepared using AiO (top row) and DD (bottom row) fabrication methods with light delivery achieved using a,d) end-on, b,e) through-fiber, and c,f) side-on illumination, respectively.

The ultrasound generation performance of the CSNP-PDMS composite-coated fibers was measured and the results are summarized in **Table 1**. The average peak-to-peak pressure generated by the CSNP-PDMS composites fabricated using DD and AiO methods are similar 2.77 ± 0.49 and 2.73 ± 0.38 MPa, respectively, with maximum respective peak-to-peak pressures achieved of 3.4 and 3.2 MPa (Figure 4b). Moreover, irrespective of the composite fabrication route, all coated fibers achieved wide ultrasound bandwidths (Figure 4c); CSNP-PDMS composites fabricated using bi-layer DD methods (30.30 ± 1.80 MHz) were similar to those yielded from the AiO composites (28.95 ± 1.24 MHz) as shown by their respective standard deviations. Ultrasound generation efficiencies calculated for CSNP-PDMS composites fabricated using both the AiO and DD methods were 0.031 ± 0.005 and 0.036 ± 0.008 MPa mJ^{-1} cm^{-2}, respectively, with a maximum generation efficiency of 0.048 MPa mJ^{-1} cm^{-2} recorded for a "DD" CSNP-PDMS sample (Table 1).

5.3. All-Optical Ultrasound Imaging

Using the point-spread-functions (Figure S8a,b, Supporting Information) recorded from the synthetic aperture of imaging the tungsten wire phantom, axial imaging resolutions as low as 40 µm (**Figure 5**b) were measured and illustrated in the high-resolution OpUS images of the tungsten wire phantom (Figure 5a). The axial imaging resolutions varied slightly over depths from 3 to 14 mm. The maximum and minimum axial resolutions were measured at 60 and 40 µm at depths of 4 and 7 mm, respectively. The corresponding lateral imaging resolution remained larger than that of the axial resolution at all imaging depths, increasing linearly along with the increasing imaging depths, rising from a minimum of 180 µm at a 3 mm imaging depth, to 260 µm at a depth of 14 mm.

A CSNP-PDMS-coated ultrasound transmitter fabricated through the DD method was used to image ex vivo tissue correlating to two distinct lamb brain regions, the cerebrum (**Figure 6**b) and cerebellum (Figure 6c). For both brain region samples, the outer surface of the tissue was well-resolved across the whole sample and the corresponding dynamic ranges were 42 dB (cerebrum) and 41 dB (cerebellum). Interestingly, the ultrasound image showed the cerebrum surface as a bright region with a well-defined and smooth morphology, whereas the surface of the cerebellum was similar in appearance to the bulk tissue. The OpUS imaging for both ex vivo brain tissue clearly showed the overall corresponding tissue shape, with contours following the brain surface (shown in Figure 6b,c by the blue arrows).

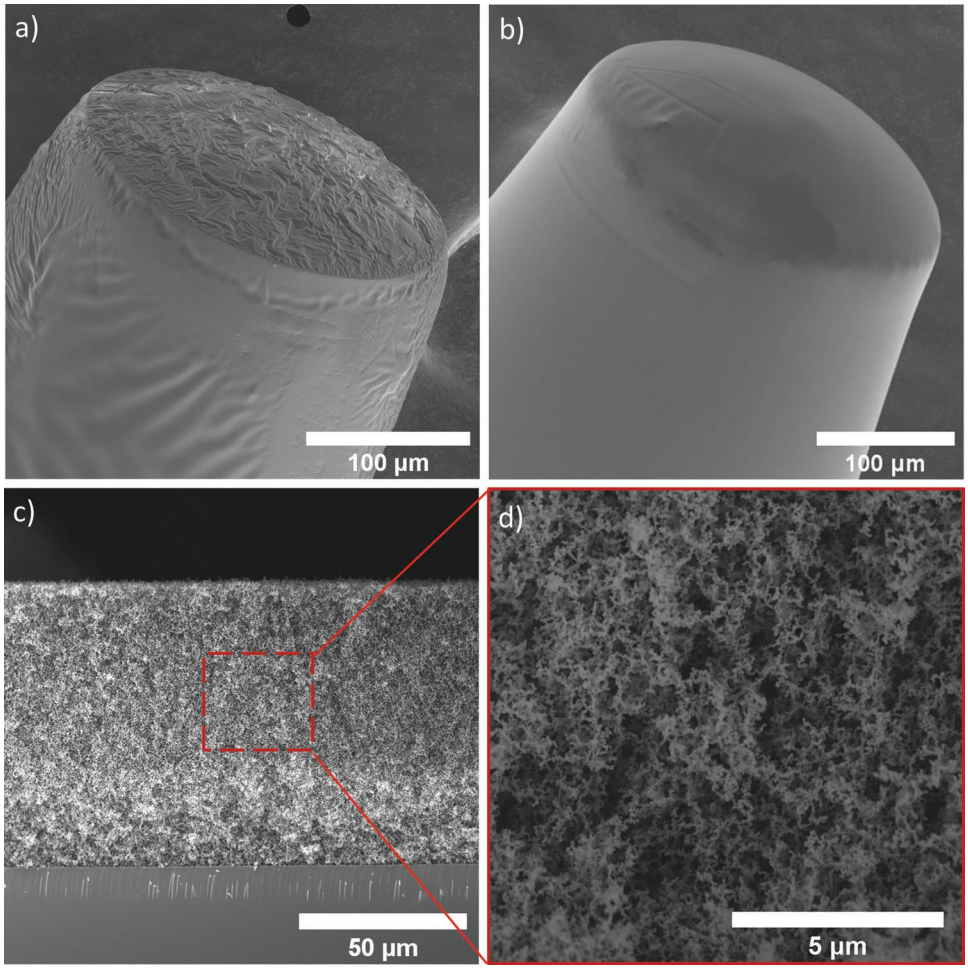

Figure 3. Scanning electron microscopy (SEM) images of the CSNP-PDMS fiber-optic coatings fabricated using a) AiO and b) DD methods. SEM images of the CSNP nanostructure deposited onto a planar glass slide; (deposition time: 20 s), at c) lower and d) higher magnifications. a) AiO and b) DD CSNP-PDMS coatings are photographed at the same scale.

6. Discussion

In this paper, we report two methods to create CSNP-PDMS composite coatings on optical fibers to transform them into OpUS transmitters. For the first time, we report the use of an AiO fabrication method to fabricate CSNP-PDMS composites directly on optical fibers, achieving integrated, highly optical absorbing coatings with small thicknesses. We also report the use of a DD method to create bilayer CSNP-PDMS composites on optical fibers. Both AiO and DD techniques showed

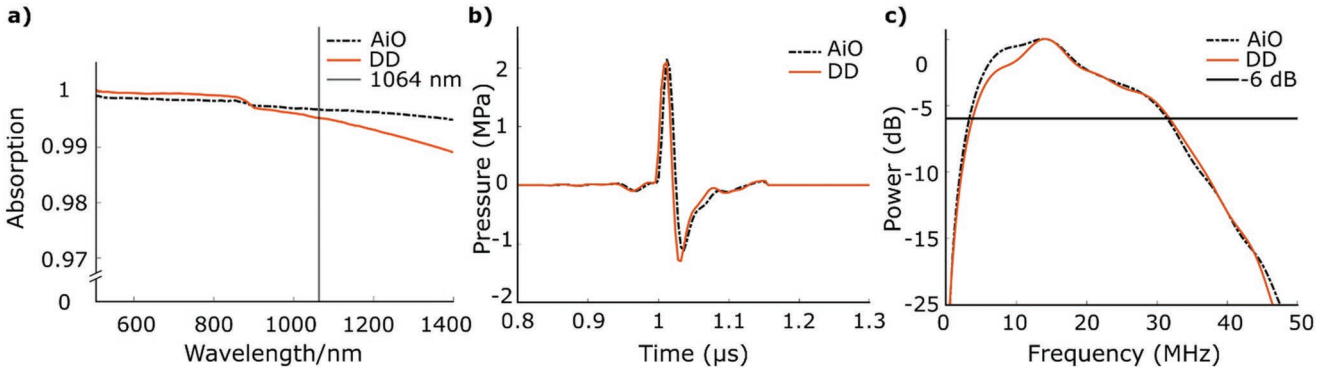

Figure 4. a) Absorption spectra for CSNP-PDMS films developed using AiO (black dashed line) and DD (orange solid line) methods with a black line illustrating absorption at 1064 nm. b) Ultrasound wave plots and c) power spectra of CSNP-PDMS films fabricated by AiO (black dashed line) and DD (orange solid line) methods. The black line in the power spectra describes the bandwidth at –6 dB.

Table 1. Ultrasound pressures, bandwidths, and generation efficiencies of CSNP-PDMS fiber-optic transmitters fabricated with the AiO and DD methods including the mean values with standard deviations (S.D.) and maximum measurements with the maximum ultrasound pressure describing the peak-to-peak maximum pressures. Averages were calculated from measurements from multiple transmitters fabricated using the DD and AiO fabrication strategies.

Method	Ultrasound pressure [MPa]			Ultrasound bandwidth [MHz]			OpUS generation efficiency [MPa mJ^{-1} cm^{-2}]		
	Mean	S.D.	Maximum	Mean	S.D.	Maximum	Mean	S.D.	Maximum
AiO	2.7	0.4	3.3	29.0	1.2	31.3	0.03	0.01	0.04
DD	2.8	0.5	3.4	30.3	1.8	32.7	0.04	0.01	0.05

ultrasound pressures and bandwidths exceeding 3 MPa and 29 MHz, respectively. Using these miniature OpUS transmitters and a FP fiber-optic hydrophone, the generated ultrasound by the composites resulted in high-resolution B-mode images of lamb brain cerebellum and cerebrum tissue, revealing subsurface features and clinically relevant imaging resolutions

Accounting for differences in experimental setups, the high ultrasound pressures, broad bandwidths, and photoacoustic generation efficiencies achieved by these CSNP-PDMS coated fibers, compare favorably to other fiber-optic nanocomposite-coatings for OpUS reported in the literature such as MWCNT-PDMS,[9,25] gold NP-PDMS,[11,35] $CuInS_2$ quantum dot-PDMS,[36] and graphite-epoxy.[56] Both CSNP-PDMS composites exhibited complete and uniform coverage of the fiber end-faces along with high optical absorbances at wavelengths across the detector bandwidth. This contrasts with the coffee-ring staining observed when solution-based methods were used to deposit MWCNTs onto fiber-optic end-faces to develop MWCNT-PDMS composites, which was previously mitigated through the complicated development of a MWCNT-gel resulted in more

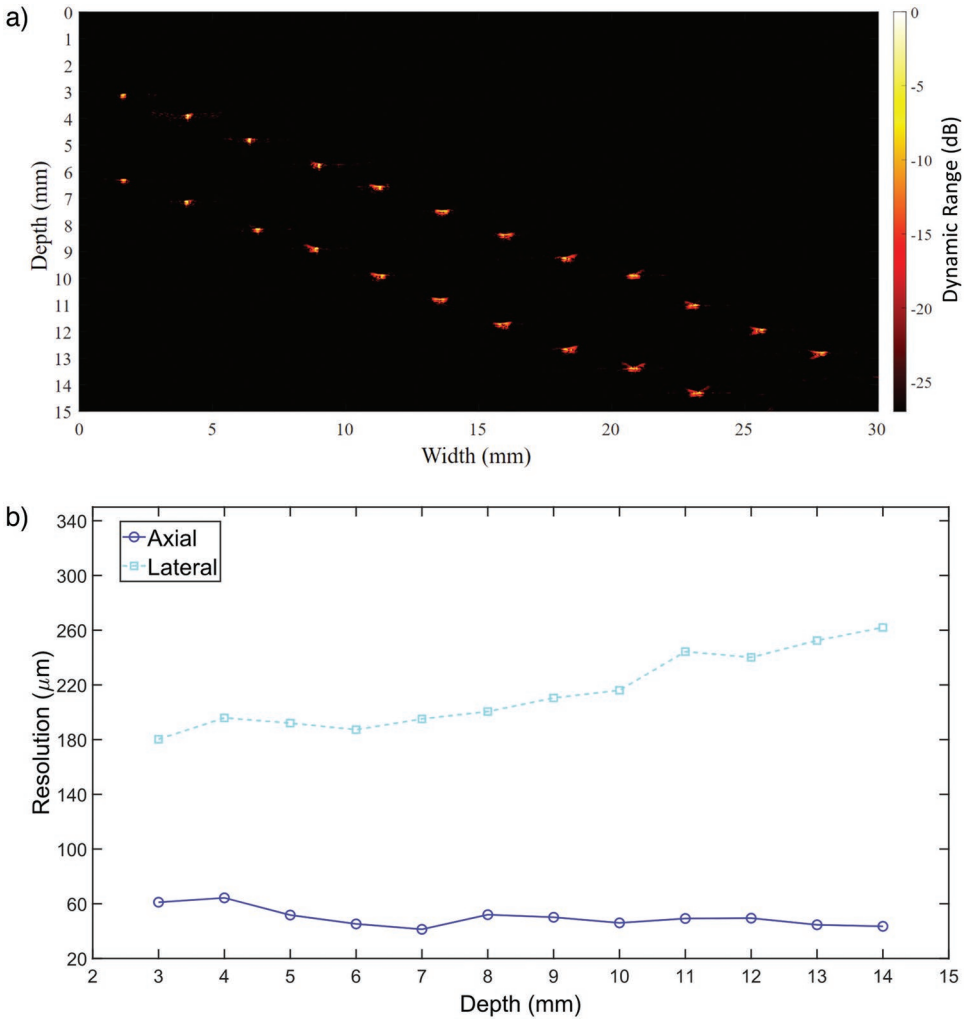

Figure 5. a) Pulse-echo ultrasound image of a tungsten wire array phantom and b) the corresponding axial and lateral resolutions measured at different depths.

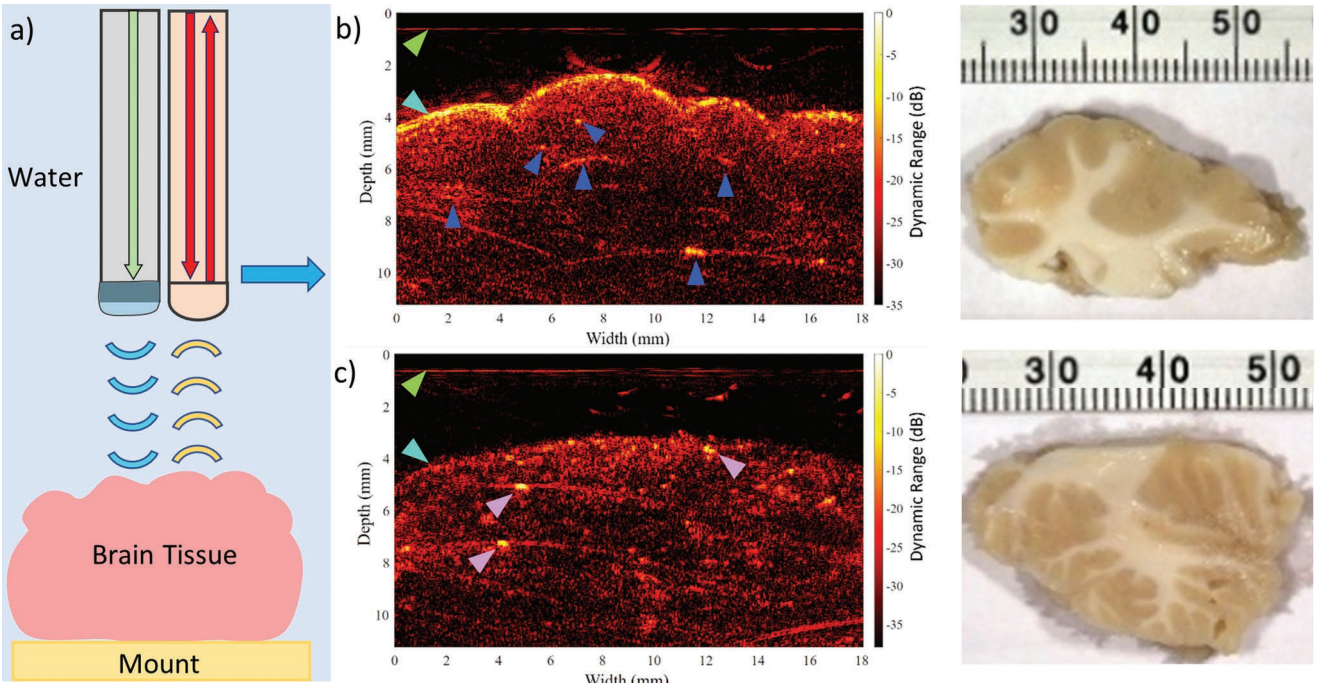

Figure 6. OpUS tissue imaging set-up located in a) a water bath consisting of a CSNP-PDMS fiber-optic OpUS transmitter with a pulsed 1064 nm (green arrow) wavelength alongside a fiber-optic FP sensor interrogated using the CW laser (1500–1600 nm, red arrows). The transducer probe images a piece of brain tissue, affixed to a corkboard mount, travelling laterally across the tissue. Pulse-echo ultrasound images of longitudinal sections of the b) cerebrum and c) cerebellum along with microscope photos of the imaged brain tissue shown to the right of each of its corresponding ultrasound image. Green arrows point to ultrasound cross-talk, the blue arrows highlight the tissue surface, and the dark blue and purple arrows indicate subsurface regions in the cerebrum and cerebellum, respectively, which could correspond to biological matter.

uniform surface coverage.[25] The fiber-optic composite fabricated with the DD method exhibited a smoother coverage than the composite produced using the AiO method, which features a more textured surface morphology. This most likely results from the mixing of the PDMS and CSNPs in the AiO methodology leading to CSNPs being located at the surface of the resulting fiber-optic composite. Whereas, in the DD method, the CSNP layer is completely covered with a PDMS overcoat, limiting the number of CSNPs that feature at the composite's surface resulting in the smooth appearance provided by the PDMS. Moreover, the generated ultrasound pressures of CSNP-PDMS composites created using both fabrication methods remained stable over time periods relevant to proposed minimally invasive interventions, decreasing in amplitude by 13.24% and 19.03% for the AiO and DD-fabricated composites, respectively, over a 3-h timeframe. These measurements demonstrate the photostability of the CSNP-PDMS composites (Figure S9, Supporting Information). We did not observe any visible damage (or a decrease in the acoustic signal which is an indication of damage assuming the composite is photostable) on the composite at the laser fluence of 80 mJ cm^{-2}. In previous work using a similar composite, Faraz et al. reported a damage threshold of 54.3 mJ cm^{-2}.[46] The improvement in the damage threshold here may be due to larger thickness of the composites fabricated in this study (>51 µm) compared to that produced by Faraz et al. (40 µm).[46] Taking these advantages and generated acoustic characteristics (Figure 4) into account, CSNPs can be considered as an alternative optical absorber to MWCNT; which present toxicity concerns over their asbestos-like aspect ratios, are expensive to manufacture and have far more complicated syntheses[57,58]

The average acoustic pressures, bandwidths, and efficiencies measured from composites produced using the DD and AiO each lie within the other method's corresponding standard deviation. For this reason, both fabrication methods can be applied as preferred by application for designing fiber-optic ultrasound transmitters.

Previously, Faraz et al. outlined a method for the synthesis of an integrated CSNP-PDMS composite, whereby CSNPs were mixed with PDMS in different ratios and deposited via drop-casting onto macroscale planar substrates.[46] Relative to that study, there are important differences in the results presented in this work. The AiO fabrication route described in this study involves a CSNP-PDMS formulation featuring a significantly higher proportion (>2.7 times larger) of CSNPs than those reported in Faraz et al.[46] This formulation was prepared without the use of a solvent, providing homogenous composites with an even distribution of CSNPs. It could be surmised that the greater inclusion of CSNPs into the AiO composites could provide a shorter absorption length leading to higher ultrasound pressures and wider ultrasound bandwidths generated. The fiber-optic CSNP-PDMS composites produced in this study generated wider bandwidths (>29 MHz) than those measured from the planar CSNP-PDMS composites fabricated in Faraz et al. (13.62 MHz).[46] Additionally, the AiO CSNP-PDMS composites described in this work were applied directly to fiber-optic distal ends, which thereby presents different challenges to depositing macroscale films, and requires separate

deposition methods, such as dip coating. Further, a comparison with another method for fabricating fiber-optic CSNP-PDMS composites (DD method) has been performed and the AiO method has shown to provide composites with very similar ultrasound pressures and bandwidths.

As a future study, optimization of the AiO and DD fabrication routes could be carried out to provide greater control of the thickness and homogeneity of the CSNP-PDMS composites can be investigated. Furthermore, to improve consistency in coating thickness, the correlation between the optical absorption and the thickness of the deposited CSNP can be explored spectroscopically. In particular, it can be advantageous to better control the thickness of the CSNP-contained optically absorbing region as generated ultrasound can undergo acoustic attenuation when the optical thicknesses are beyond the optical penetration depth. In this context, for the DD approach, a mechanical shutter placed in between the flame and the fiber could be employed. Alternatively, the fiber could be moved into the flame at a certain distance for a set period and then removed using a motorized stage. For the sake of improving transmitter efficiency further, for the AiO method, diluting the PDMS formulation can be considered to decrease acoustic attenuation. This can not only optimize coating thickness with respect to the optical penetration depth for AiO methods but lead to greater pressures and bandwidths. Introducing a solvent into the reaction mixture for dilution would not only lead to a lower viscosity composite solution, but residual solvent would evaporate from the applied coating leading to a thinner composite. Further, the mixing of the CSNPs and PDMS using a solvent might reduce aggregation of the CSNPs, thereby providing a greater degree of integration between the CSNPs and PDMS causing a composite with a higher heat transfer rate. However, overly reducing the PDMS-solvent ratio could lead to a composite thinner than that of the laser penetration depth causing some of the incident laser light to be transmitted through the composite. This would then lower the optical energy absorbed and the subsequent thermal energy accrued and reducing the generated ultrasound pressures.

The effect of different candle wick materials and dimensions, flame temperatures, and flame-substrate separations may affect candle-soot production.[59] Thus, the effect of each factor on the ultrasound generation should be examined to standardize the coatings-development methods further. Furthermore, for use as image guidance for minimally invasive surgical interventions, whilst many studies have concluded that CSNPs possess low toxicities[59,60] or are non-toxic[58] nevertheless, CSNP-PDMS nanocomposites would require leaching studies to ensure that the CSNPs would not seep from the elastomeric matrix either under prolonged (>3 h) in vivo use during or in storage between (>3 days) surgical interventions. It is not envisaged that the CSNPs would leach from the surrounding PDMS as for AiO coatings, the CSNPs are fully encapsulated within a PDMS layer and for DD coatings, the CSNP layer is not only fully integrated with PDMS infiltrating the mesh-like structure but also, over-coated with a layer of bulk PDMS. However, to examine the stability of the nanocomposites with respect to leaching under physiological conditions, further studies should be undertaken.

In our study, the high ultrasound pressures generated by these miniature devices enabled B-mode ultrasound imaging of a wire phantom (with depths of up to 12 mm) as well as ex vivo lamb brain tissue, with imaging depths of over 8 mm. The recorded signal at these depths exhibited a large dynamic range indicating that imaging at larger depths is likely possible. Furthermore, the wide ultrasound bandwidths resulted in high-resolution ultrasound imaging of the wire phantom, characterized by the high axial resolutions of 40 µm. At all imaging depths, the achieved lateral resolution remained lower than that of the axial resolution, which is estimated to be largely due to limited view artifacts and the directivity of the fiber-optic imaging transducer probe. The ex vivo ultrasound imaging of the lamb brain tissue demonstrates the potential for applications where distinguishing small physiological features is necessary. This study leaves open a detailed exploration of the histo-pathological correlates of the OpUS images of brain tissue, which could include an investigation of the highly echogenic subsurface features observed here. If verified ultrasound images of cross sections of lamb cerebellum and cerebrum could be used as references, the features resolved in the B-mode ultrasound images of the brain tissue could perhaps be assigned to particular structures within the brain. Brain tissue is largely soft with similar echogenicity, resulting in low ultrasound contrast, which presents challenges when resolving features such as white and grey matter.[61] However, this imaging study illustrated the high-resolution biological imaging performance and large dynamic range demonstrated by the OpUS devices, enabling the visualization of several distinct features within the brain tissue. This highlights the potential of CSNP-PDMS nanocomposites for minimally invasive all-OpUS imaging as demonstrated by the all-optical B-mode ultrasound images of a lamb cerebellum and cerebrum. Several minimally invasive surgical procedures such as deep-brain stimulation[62,63] and tumor biopsy[64,65] require ultrasound imaging guidance and miniaturized OpUS transducers have strong potential to guide neurological surgical interventions in these contexts.

CSNP-PDMS fiber-optic OpUS transmitters, engineered through two distinct reproducible fabrication routes, demonstrated clinically useful peak-peak ultrasound pressures (>3 MPa) and bandwidths (>29 MHz) and performed ex vivo imaging of brain tissue at deep imaging depths of beyond 8 mm. These results show that miniaturized OpUS transducers have strong potential to be integrated with the devices that are used in neurological interventions[62–65] and to provide structural information to surgeons.

Conflict of Interest

R.J. Colchester and A.E Desjardins declare a conflict of interest with both parties owning shares in Echopoint Medical Ltd.

Data Availability Statement

The data that support the findings of this study are available from the corresponding author upon reasonable request.

Supporting Information

Supporting Information is available from the Wiley Online Library or from the author.

Keywords

brain imaging, candle soot nanoparticles, optical fibers, optical ultrasound, polydimethylsiloxane

Received: August 12, 2022
Revised: November 30, 2022
Published online: February 24, 2023

[1] N. J. Dawson, M. G. Kuzyk, J. Neal, P. Luchette, P. Palffy-Muhoray, in SPIE Organic Photonics + Electronics, Vol. *8475*, SPIE, Bellingham, WA **2012**, p. 84750B.
[2] M. Corbaci, W. Walter, K. Lamkin-Kennard, *Actuators* **2018**, *7*, 73.
[3] J. Loomis, X. Fan, F. Khosravi, P. Xu, M. Fletcher, R. W. Cohn, B. Panchapakesan, *Sci. Rep.* **2013**, *3*, 1900.
[4] C. Tyagi, A. Sharma, in AIP Conf. Proceedings, Vol. *1675*, American Institute of Physics, New York **2015**, p. 030055.
[5] D. Godovsky, L. Chen, L. Pettersson, O. Ingana, M. R. Andersson, J. C. Hummelen, *Adv. Mater. Opt. Electron.* **2000**, *10*, 47.
[6] H. Chen, C. Lin, H. Han, K. Chen, Y. Tsai, Y. Chang, M. Shih, H. Kuo, P. S. Yu, *Sol. Energy Mater. Sol. Cells* **2012**, *104*, 92.
[7] J. Ozhikandathil, M. Packirisamy, in Photonics North 2010, Vol. *7750*, SPIE, Bellingham, WA **2010**, p. 775004.
[8] S. M. Briglin, N. S. Lewis, *J. Phys. Chem. B* **2003**, *107*, 11031.
[9] R. J. Colchester, E. Z. Zhang, C. A. Mosse, P. C. Beard, I. Papakonstantinou, *Biomed. Opt. Express* **2015**, *6*, 1502.
[10] R. J. Colchester, C. Little, G. Dwyer, S. Noimark, E. J. Alles, E. Z. Zhang, C. D. Loder, I. P. Parkin, I. Papakonstantinou, P. C. Beard, M. C. Finlay, R. D. Rakhit, A. E. Desjardins, *Sci. Rep.* **2019**, *9*, 1.
[11] S. Noimark, R. J. Colchester, R. K. Poduval, E. Maneas, E. J. Alles, T. Zhao, E. Z. Zhang, M. Ashworth, E. Tsolaki, A. H. Chester, N. Latif, S. Bertazzo, A. L. David, S. Ourselin, P. C. Beard, I. P. Parkin, I. Papakonstantinou, A. E. Desjardins, *Adv. Funct. Mater.* **2018**, *28*, 1704919.
[12] T. Zhao, L. Su, W. Xia, *J. Healthcare Eng.* **2018**, *2018*, 1.
[13] S.-L. Chen, *Appl. Sci.* **2016**, *7*, 25.
[14] E. J. Alles, R. J. Colchester, A. E. Desjardins, *IEEE Trans. Ultrason. Ferroelectr. Freq. Control* **2016**, *63*, 83.
[15] E. J. Alles, N. F. Sheung, S. Noimark, E. Z. Zhang, P. C. Beard, A. E. Desjardins, *Sci. Rep.* **2017**, *7*, 1.
[16] G. Wissmeyer, M. A. Pleitez, A. Rosenthal, V. Ntziachristos, *Light: Sci. Appl.* **2018**, *7*, 53.
[17] E. J. Alles, S. Noimark, E. Maneas, E. Z. Zhang, P. C. Beard, A. E. Desjardins, I. P. Parkin, *Biomed. Opt. Express* **2018**, *9*, 3481.
[18] J. Kim, W. Y. Chang, H. Wu, X. Jiang, in 2017 IEEE Int. Ultrasonics Symp. (IUS), IEEE, Piscataway, NJ **2017**, pp. 1–4.
[19] J. Kim, H. Kim, W. Y. Chang, W. Huang, X. Jiang, P. A. Dayton, *IEEE Nanotechnol. Mag.* **2019**, *13*, 13.
[20] R. J. Colchester, E. J. Alles, A. E. Desjardins, *Appl. Phys. Lett.* **2019**, *114*, 113505.
[21] R. J. Colchester, C. D. Little, E. J. Alles, A. E. Desjardins, *OSA Continuum* **2021**, *4*, 2488.
[22] K. Pham, S. Noimark, N. Huynh, E. Zhang, F. Kuklis, J. Jaros, A. Desjardins, B. Cox, P. Beard, *IEEE Trans. Ultrason. Ferroelectr. Freq. Control* **2020**, *68*, 1007.
[23] T. Buma, M. Spisar, M. O'Donnell, *IEEE Trans. Ultrason. Ferroelectr. Freq. Control* **2003**, *50*, 1161.
[24] Y. Hou, J.-S. Kim, S. Ashkenazi, M. Donnell, L. J. Guo, *Appl. Phys. Lett.* **2006**, *89*, 093901.
[25] S. Noimark, R. J. Colchester, B. J. Blackburn, E. Z. Zhang, E. J. Alles, S. Ourselin, P. C. Beard, I. Papakonstantinou, I. P. Parkin, A. E. Desjardins, *Adv. Funct. Mater.* **2016**, *26*, 8390.
[26] N. Wu, X. Zou, J. Zhou, X. Wang, *Measurement* **2016**, *79*, 164.
[27] R. K. Poduval, S. Noimark, R. J. Colchester, T. J. Macdonald, I. P. Parkin, A. E. Desjardins, I. Papakonstantinou, *Appl. Phys. Lett.* **2017**, *110*, 223701.
[28] S. Zhang, E. Z. Zhang, P. C. Beard, A. E. Desjardins, R. J. Colchester, *Commun. Eng.* **2022**, *1*, 20.
[29] R. Colchester, E. Zhang, P. Beard, A. Desjardins, *Biomed. Opt. Express* **2022**, *13*, 4047.
[30] M. C. Finlay, C. A. Mosse, R. J. Colchester, S. Noimark, E. Z. Zhang, S. Ourselin, P. C. Beard, R. J. Schillin, I. P. Parkin, I. Papakonstantinou, A. E. Desjardins, *Light: Sci. Appl.* **2017**, *6*, e17103.
[31] R. J. Colchester, C. A. Mosse, D. S. Bhachu, J. C. Bear, C. J. Carmalt, I. P. Parkin, B. E. Treeby, I. Papakonstantinou, A. E. Desjardins, R. J. Colchester, C. A. Mosse, D. S. Bhachu, J. C. Bear, C. J. Carmalt, I. P. Parkin, B. E. Treeby, I. Papakonstantinou, A. E. Desjardins, *Appl. Phys. Lett.* **2014**, *104*, 173502.
[32] T. Buma, M. Spisar, M. O'Donnell, *Appl. Phys. Lett.* **2001**, *79*, 548.
[33] S. H. Lee, Y. Lee, J. J. Yoh, *Appl. Phys. Lett.* **2015**, *106*, 081911.
[34] X. Zou, N. Wu, Y. Tian, X. Wang, *Opt. Express* **2014**, *22*, 18119.
[35] N. Wu, Y. Tian, X. Zou, X. Wang, in SPIE Smart Structures and Materials + Nondestructive Evaluation and Health Monitoring, Vol. *8694*, SPIE, Bellingham, WA **2013**, p. 86940Q.
[36] S. Bodian, R. J. Colchester, T. J. Macdonald, F. Ambroz, M. B. de Gutierrez, S. J. Mathews, Y. M. M. Fong, E. Maneas, K. A. Welsby, R. J. Gordon, P. Collier, E. Z. Zhang, P. C. Beard, I. P. Parkin, A. E. Desjardins, S. Noimark, *Adv. Mater. Interfaces* **2021**, *8*, 2100518.
[37] J. A. Guggenheim, J. Li, T. J. Allen, R. J. Colchester, S. Noimark, O. Ogunlade, I. P. Parkin, I. Papakonstantinou, A. E. Desjardins, E. Z. Zhang, P. C. Beard, *Nat. Photonics* **2017**, *11*, 714.
[38] E. Z. Zhang, P. C. Beard, in SPIE BiOS, Vol. *7899*, SPIE, Bellingham, WA **2011**, p. 78991F.
[39] W.-Y. Chang, W. Huang, J. Kim, S. Li, X. Jiang, *Appl. Phys. Lett.* **2015**, *107*, 161903.
[40] Y. Guo, H. W. Baac, S.-L. Chen, T. B. Norris, L. J. Guo, in SPIE BiOS, Vol. *7899*, SPIE, Bellingham, WA **2011**, p. 78992C.
[41] B.-Y. Hsieh, J. Kim, J. Zhu, S. Li, X. Zhang, X. Jiang, *Appl. Phys. Lett.* **2015**, *106*, 021902.
[42] B. Zhang, D. Wang, B. Yu, F. Zhou, W. Liu, *RSC Adv.* **2014**, *4*, 2586.
[43] C. Yang, Z. Li, Y. Huang, K. Wang, Y. Long, Z. Guo, X. Li, H. Wu, *Nano Lett.* **2021**, *21*, 3198.
[44] W. Y. Chang, X. A. Zhang, J. Kim, W. Huang, A. Bagal, C. H. Chang, T. Fang, H. F. Wu, X. Jiang, *IEEE Trans. Nanotechnol.* **2018**, *17*, 985.
[45] Y. Li, Z. Guo, G. Li, S.-L. Chen, *Opt. Express* **2018**, *26*, 21700.
[46] M. Faraz, M. A. Abbasi, P. Sang, D. Son, *Micromachines* **2020**, *11*, 1.
[47] W. Y. Chang, X. Jiang, in 2018 IEEE 18th Int. Conf. on Nanotechnology (IEEE-NANO), IEEE, Piscataway, NJ **2018**, pp. 1–2.
[48] E. Aytac-Kipergil, E. J. Alles, H. C. Pauw, J. Karia, S. Noimark, A. E. Desjardins, *Opt. Lett.* **2019**, *44*, 6005.
[49] R. O. Illing, J. E. Kennedy, F. Wu, G. R. ter Haar, A. S. Protheroe, P. J. Friend, F. v. Gleeson, D. W. Cranston, R. R. Phillips, M. R. Middleton, *Br. J. Cancer* **2005**, *93*, 890.
[50] S. Dromi, V. Frenkel, A. Luk, B. Traughber, M. Angstadt, M. Bur, J. Poff, J. Xie, S. K. Libutti, K. C. P. Li, B. J. Wood, *Clin. Cancer Res.* **2007**, *13*, 2722.
[51] S. T. Kang, C. K. Yeh, *Langmuir* **2011**, *27*, 13183.
[52] S. Y. Yeo, A. J. A. Moreno, B. van Rietbergen, N. D. ter Hoeve, P. J. van Diest, H. Grüll, *J. Ther. Ultrasound* **2015**, *3*, 1.
[53] J. Hindley, L. Regan, E. Stewart, C. Tempany, K. Hynnen, Y. Inbar, K. Kim, J. Geschwind, G. Hesley, B. Gostout, M. Sklair-Levy, *Am. J. Roentgenol.* **2004**, *183*, 1713.
[54] E. J. Alles, R. J. Colchester, A. E. Desjardins, in 2018 IEEE Int. Ultrasonics Symp. (IUS), IEEE, Piscataway, NJ **2018**, p. 1–9.
[55] B. E. Treeby, B. T. K.-W. Cox, *J. Biomed. Opt.* **2010**, *15*, 021314.

[56] E. Biagi, F. Margheri, D. Menichelli, *IEEE Trans. Ultrason. Ferroelectr. Freq. Control* **2001**, *48*, 1669.
[57] H.-J. Eom, J.-S. Jeong, J. Choi, *Environ. Health Toxicol.* **2015**, *30*, e2015001.
[58] S. Ahlawat, A. Singh, S. K. Sharma, P. K. Mukhopadhyay, R. Singh, K. S. Bindra, *Surf. Topogr.: Metrol. Prop.* **2020**, *8*, 025007.
[59] M. R. Mulay, A. Chauhan, S. Patel, V. Balakrishnan, A. Halder, R. Vaish, *Carbon* **2019**, *144*, 684.
[60] H. Pandey, S. Saini, S. P. Singh, N. K. Gautam, S. Singh, *Comp. Biochem. Physiol., Part C: Toxicol. Pharmacol.* **2020**, *228*, 108646.
[61] P. Clarke, P. Muthukumar, *Joint Trust Guideline for Cranial Ultrasound Scanning of Infants in NICU*.
[62] R. Nayak, J. Lee, S. Chantigian, M. Fatemi, S. Y. Chang, A. Alizad, *Phys. Med. Biol.* **2021**, *66*, 0.
[63] H. Zhou, L. Niu, L. Meng, Z. Lin, J. Zou, X. Xia, X. Huang, W. Zhou, T. Bian, H. Zheng, *Research* **2019**, *2019*, 1.
[64] A. Dizeux, M. Gesnik, H. Ahnine, K. Blaize, F. Arcizet, S. Picaud, J. A. Sahel, T. Deffieux, P. Pouget, M. Tanter, *Nat. Commun.* **2019**, *10*, 1.
[65] J. Mung, F. Vignon, R. Erkamp, D. Stanton, A. Jain, *2013 IEEE Int. Ultrasonics Symp. (IUS)*, IEEE, Piscataway, NJ **2013**, pp. 2053–2056.